Article:
Homan, S., Mac Dowell, N. and Brown, S. (2021) Grid frequency volatility in future low inertia scenarios: challenges and mitigation options. Applied Energy, 290. 116723. ISSN: 0306-2619

https://doi.org/10.1016/j.apenergy.2021.116723

Grid frequency volatility in future low inertia scenarios: challenges and mitigation options

Samuel Homan[a], Niall Mac Dowell[b], Solomon Brown[a,*]

[a] *Department of Chemical and Biological Engineering, University of Sheffield, Sheffield, S1 3JD, UK*
[b] *Centre for Environmental Policy, Imperial College London, London, SW7 1NA, UK*

Abstract

Electricity grids across the world are rapidly changing to accommodate an increasing penetration of renewable generation, but concerns have been raised about the stability of grids during and after this transition. The volatility of the frequency of the grid is a commonly used metric for stability. Here we analyse historic frequency data from Great Britain to gain an understanding of the past and current state of frequency volatility and some of the driving forces behind patterns and trends. We show that frequency volatility increased appreciably in 2017 and 2018. Using predicted 2030 inertia profiles, we also determine the future frequency response requirements of the grid in two different situations: after a large infeed loss and during normal day-to-day operation. In normal day-to-day operation, the frequency volatility does not drastically deteriorate until an inertia level around 20% of current levels (inertia from nuclear and demand only). At this low level, a significant portion of the frequency response capacity needs to be fast acting for successful mitigation. Increasing the capacity of slow acting response alone is actually found to be detrimental. Low inertia has a much greater effect on frequency response requirements in a large infeed loss situation.

Keywords: Grid stability, Grid inertia, Renewable energy, Fast frequency response.

1. Introduction

Maintaining a stable grid is one of the top priorities of electricity system operators (ESOs) [1, 2]. One measure of grid stability is the volatility of the AC frequency of the grid, the frequency at which all synchronously connected generators and demand units rotate at. Frequency deviations reflect the imbalance between generation and demand: when generation is greater than demand, the frequency rises and vice versa. ESOs balance generation and demand on a second-by-second basis to maintain a frequency as close to the nominal value as possible, achieved through frequency response (FR) services. FR is provided by generation and demand units that can alter their power input or output in response to changes in the grid frequency. FR, along with voltage regulation,

*Corresponding author
Email address: s.f.brown@sheffield.ac.uk (Solomon Brown)

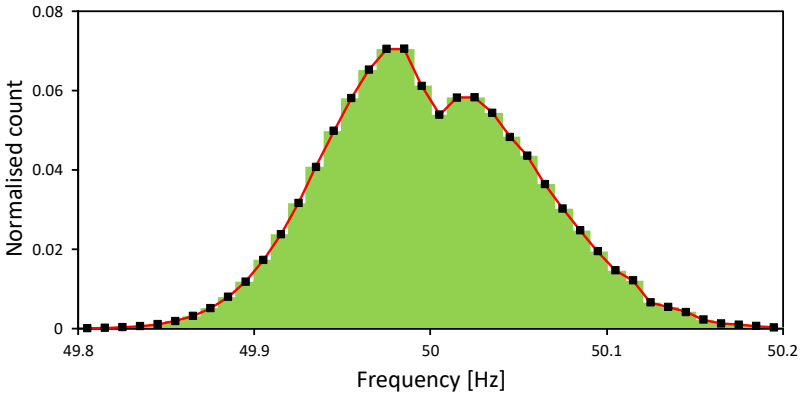

Figure 1: Distribution of grid frequency in GB (2014–2018). Bin width: 0.01 Hz.

reserve, and system restoration is an important ancillary service which is necessary in all large-scale grids around the world. As an example, Fig. 1 shows the distribution of grid frequency in Great Britain (GB) for 2014–2018, indicating that in the vast majority of times this balancing act is successful because deviations outside of ±0.2 Hz of the nominal frequency are very rare (0.06% of the time).

Very occasionally, unexpected events can cause large frequency deviations that require demand disconnection to restore balance (i.e. blackouts). Blackouts are costly, dangerous, and cause serious disruption. The most recent severe event in GB, caused by the simultaneous loss of multiple generators, occurred on August 9$^{\text{th}}$ 2019 and resulted in a loss of power for approximately 1 million customers [3]. In 2003, large-scale blackouts caused by generator losses occurred in North America and continental Europe [4], and in 2016 tornadoes caused the South Australian grid to become separated (islanded) from the national system and subsequently lost to a blackout [5].

The rate of change of frequency (RoCoF) after an imbalance between generation and demand is inversely proportional to the amount of inertia in the grid [6]. The large rotating masses in a thermal plant are the main providers of inertia on the generation side, and there is also a significant contribution to inertia from the demand side. Many forms of renewable generation, particularly wind and solar, offer very little (or zero) inertia to the grid either due to being connected via power electronics or because they have no inherent inertia for lack of moving parts. Wind and solar are also intermittent and non-dispatchable forms of generation, so they cannot load follow.

As part of strategies to meet climate change targets [7, 8], electricity grids around the world are decarbonising [9]. In GB, there has been an increase in the proportion of electricity generated via wind and solar over the last several years, from a 7% share in 2010 to a 29% share in 2017 [10]. This trend will almost certainly continue, with predictions of a 60% share by 2025 [11]. This has raised concerns about the effect that increasing penetrations of wind and solar have on grid stability. As inertia reduces, FR becomes increasingly important for maintaining a stable frequency, and

GB's ESO has recognised the need to review its current FR services [12] to ensure they are fit for purpose in a future grid.

A brief review on previous work on reduced inertia in power systems, and mitigation strategies, is provided as follows. Ulbig et al. [13] derived the swing equation [6] for interconnected power systems, and studied the impacts of low inertia on the continental European grid. Tielens et al. [14] reviewed the relevance of inertia in power systems and discussed synthetic inertia (SI) as a replacement, amongst others. Fast acting FR is an alternative to SI [15], and was found to be effective, provided the ramp time is short enough [16]. Lee et al. [17] and Greenwood et al. [18] investigated how energy storage can fulfil the need for fast acting FR in low inertia systems. Johnson et al [19] used unit commitment and dispatch modelling to quantify the amount of inertia in the Texas grid in future scenarios and in a later publication [20] the authors investigated the feasibility of extremely high penetrations of renewables and identified mitigation pathways. They found that low inertia could prevent a 100% penetration. In terms of mitigation, reducing the size of the largest loss was found to be more impactful than fast acting FR. Vorobev et al. [21] presented a method for finding the probability density function of the frequency of a power system. They used their method to uncover key system parameters influencing frequency dynamics, and found that inertia has little effect on the frequency probability density function.

The existing literature contains a large number of studies on the effect of reduced inertia on frequency volatility after a single large infeed loss (LIL) situation, see for example [22, 23]. There are far fewer investigations into the effects on normal day-to-day frequency volatility, but there is some research that suggests the effects are minimal [21]. To fill this gap in knowledge and to further existing work, this paper addresses the following research questions:

- What is the current state of frequency volatility and what are the underlying drivers behind volatility?
- What is the relationship between inertia and FR requirements in a LIL situation?
- In which future inertia scenarios does the normal day-to-day frequency volatility become unacceptable and what needs to change in FR provision to mitigate this?

To address these questions, we take the GB grid as an exemplar. To address the first question, we conduct an analysis of historic GB frequency data and investigate potential causes of patterns and trends seen in the data, building on previous work [24, 25, 26]. To address the second question, we analytically solve the swing equation (with a simplified FR model) and apply constraints based on GB frequency requirements after a LIL. To address the last question, we develop a model of the GB grid, with FR modelled based on minimum GB grid code requirements (enhancing the approach presented in [17]), which we use to estimate the power imbalance profile of an entire

month: November 2018. This month is used as a case study to investigate the FR provision necessary to maintain acceptable frequency volatility during normal day-to-day operation in future (2030) scenarios. The future scenarios considered are ones in which the inertia profiles are lower than today's due to an increasing penetration of wind and solar generation. The aim is for the results to be accurate for the GB grid specifically, but also to be relevant to other comparably sized grids on a similar decarbonisation trajectory, and the methods presented are transferable if the necessary grid data is available.

The remainder of this paper is structured as follows. Section 2 guides readers through the methodology, and Section 3 presents the results in three subsections: each one focussed on one of the research questions introduced above. Section 4 provides conclusions.

2. Methodology

In Section 2.1, we provide definitions necessary for understanding the analysis of historic GB frequency data. In Section 2.2, we introduce the swing equation [6] and in Section 2.3 use it to determine grid constraints (e.g. minimum FR capacity) for meeting certain frequency conditions after a LIL. In Section 2.4, we develop a model of the GB grid based on the swing equation. We explain how the demand and inertia input variables are acquired in Section 2.4.1 and give a detailed description of how FR is modelled in Section 2.4.2. In Section 2.4.3, we explain the use of the grid model to determine the imbalance profile of November 2018 (Nov18) and how we then use this in other simulations to investigate the change in frequency volatility when the inertia profile is varied. In Section 2.5, we explain how inertia profiles for 2030 are created.

2.1. Historic GB frequency data analysis

The analysis of historic GB frequency data is conducted using 1 s resolution data [27] from Jan 2014 to Dec 2018. The analysis focuses on frequency volatility, and two ways of measuring this are used: the number of frequency events and the frequency standard deviation. Based on the operational and statutory frequency limits in GB [28], we define 4 types of frequency event, which we use throughout this paper:

- High frequency event: frequency deviations above 50.2 Hz for any length of time
- Severe high frequency event: frequency deviations above 50.5 Hz for any length of time
- Low frequency event: frequency deviations below 49.8 Hz for any length of time
- Severe low frequency event: frequency deviations below 49.5 Hz for any length of time

Fig. 2 presents an example of a low frequency event and the definitions of event start, event end, event duration, and event magnitude.

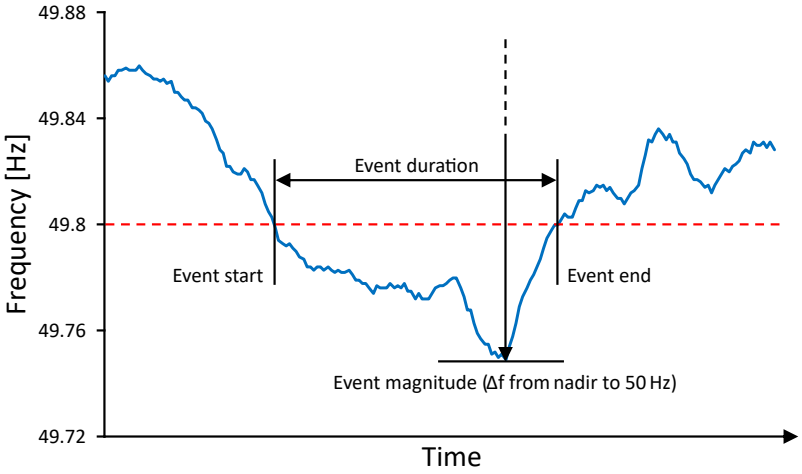

Figure 2: An example of a low frequency event, with event definitions.

2.2. Swing equation

The swing equation governs the relationship between the frequency and power imbalances on the grid [6]:

$$\frac{\mathrm{d}f}{\mathrm{d}t} = \frac{f_\mathrm{n}^2}{2E_\mathrm{n}f}(R + I - kD_\mathrm{n}\Delta f)\,. \tag{1}$$

f_n is the nominal frequency of the grid and $\Delta f = f - f_\mathrm{n}$. E_n is the total rotational kinetic energy stored in the grid at f_n, which is what we define as inertia in this paper. R is the FR of the grid, which can be positive or negative. I is the power imbalance of the grid and is positive when generation is greater than demand and negative when demand is greater than generation. Small imbalances result from continuous small fluctuations in demand or the variable output of intermittent generation whereas large imbalances are caused by unexpected generator trips, rapidly ramping interconnectors, and large demand swings. D_n is the demand at f_n. Some of the demand is frequency sensitive with a power consumption that varies with frequency (e.g. synchronous electric motors). This is a self-stabilising property of the grid and acts like instantaneous, inherent FR. The higher the value of k, the demand damping constant, the greater this effect is.

2.3. Large infeed loss

In GB, following a LIL of 1320 MW, there must be enough FR on the system to avoid frequency deviations below 49.5 Hz [29]. We shall refer to this as the frequency nadir requirement. Another requirement is that the RoCoF must not be too high following the LIL to avoid RoCoF protection relays being triggered and embedded generation tripping off the system. We shall refer to this as the RoCoF requirement. We use the swing equation (linearised with the assumption $f \approx f_\mathrm{n}$) to determine how these requirements are met.

First, the initial conditions: at $t = 0$ and $f = 50$ Hz, the LIL occurs ($I = -1320$ MW). f_n, E_n, I, k, and D_n remain constant for all time. Fig. 3 shows the frequency evolution and the FR (R)

approximated as a linear ramp after a delay. $R(t)$ has 3 stages:

$$R = \begin{cases} 0 & \text{when } t \leq t_\mathrm{d}\,, \\ R_\mathrm{cap}\frac{(t-t_\mathrm{d})}{t_\mathrm{r}} & \text{when } t_\mathrm{d} \leq t \leq t_\mathrm{d}+t_\mathrm{r}\,, \\ R_\mathrm{cap} & \text{when } t \geq t_\mathrm{d}+t_\mathrm{r}\,, \end{cases} \tag{2}$$

where t_d is the delay time between the sudden imbalance and the start of the linear ramp and t_r is the time it takes for the FR to ramp from zero to full capacity (R_cap).

The RoCoF requirement is mathematically expressed as

$$\left|\frac{\mathrm{d}f}{\mathrm{d}t}\right| \leq L_{\mathrm{f}'}\,, \tag{3}$$

where the RoCoF limit ($L_{\mathrm{f}'}$) depends on the embedded generation protection settings, and the nadir requirement is expressed as

$$\Delta f \geq L_\mathrm{f}\,, \tag{4}$$

where the nadir limit (L_f) is $-0.5\,\mathrm{Hz}$ after a $1320\,\mathrm{MW}$ loss. The RoCoF requirement gives us a constraint on the inertia:

$$E_\mathrm{n} \geq \left|\frac{f_\mathrm{n} I}{2L_{\mathrm{f}'}}\right|\,. \tag{5}$$

The steady-state frequency after a LIL must be above the nadir limit, which gives us a constraint on the FR capacity:

$$R_\mathrm{cap} \geq kD_\mathrm{n}L_\mathrm{f} - I\,. \tag{6}$$

The previous constraint must be satisfied to ensure the frequency has any chance of fulfilling the nadir requirement after a LIL. However, even with this constraint satisfied, there is still the possibility of the nadir limit being breached before or while the FR is ramping. Avoiding this possibility gives us a final constraint in the form of:

$$R_\mathrm{cap}\exp\left(\frac{At_\mathrm{r}(kD_\mathrm{n}L_\mathrm{f}-I)}{E_\mathrm{n}R_\mathrm{cap}}\right) = R_\mathrm{cap} - \frac{At_\mathrm{r}I}{E_\mathrm{n}}\exp\left(\frac{At_\mathrm{d}}{E_\mathrm{n}}\right), \tag{7}$$

where $A = kD_\mathrm{n}f_\mathrm{n}/2$. Eq. (7) can be solved for one of the FR parameters (R_cap, t_r, or t_d). The solution results in the nadir reaching, but not breaching, the nadir limit. Therefore, the solution is the absolute limit for the particular FR parameter.

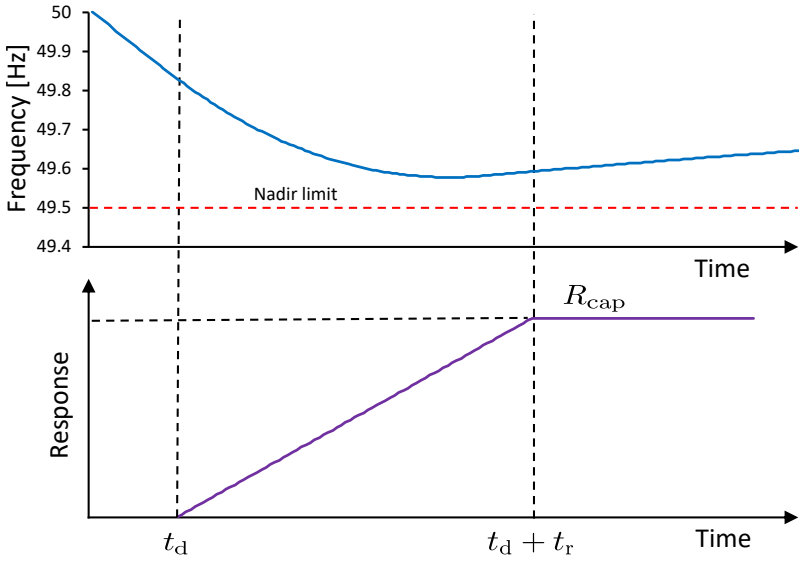

Figure 3: An example frequency profile after a large infeed loss and the frequency response approximated as a linear ramp after a delay.

2.4. GB grid model

2.4.1. Demand and inertia

The demand assumed in the GB grid model is the underlying demand (UD) of the grid: the sum of transmission connected and embedded generation and net flow of power coming into GB from interconnectors (imports minus exports), with the power used during pumped storage (PS) pumping removed. The UD is the electricity demand of all domestic, commercial, and industrial users.

To calculate UD, half-hourly data for transmission connected generation [30], interconnector imports and exports [27], and embedded wind and solar [27] is used, as well as yearly data for other embedded generation fuel types [10]. The yearly data for other embedded generation fuel types (gas, non-PS hydro, and bioenergy) is converted to a half-hourly resolution by assuming that the level of embedded generation for each fuel type is the same as their transmission connected counterpart as a percentage of their respective yearly totals. Linear interpolation is used to replace erroneous data.

The inertia of the grid is calculated using the same data sources. The total inertia of the grid (E_{n}) is the sum of contributions from the generation side ($E_{\text{n,gen}}$) and demand side ($E_{\text{n,dem}}$), which is estimated to provide 20% of the total in GB [31, 32]. Multiplying the transmission system demand (TSD), the sum of transmission connected generation and interconnector imports, by 1.75 is a simple calculation for estimating the demand inertia (and the contribution from embedded generation) [32]. Inertia from the generation side (excluding embedded generation) is calculated in a similar way to the method described in [17], using inertia constants, generation output, and

Generation type	Inertia constant, H [s]	Capacity factor, β
Combined-cycle gas turbine (CCGT)	8	0.75
Nuclear	5	0.9
Coal, biomass, and PS	4	0.75
Non-PS hydro	3	0.75
Wind, solar, and interconnectors	0	–

Table 1: Inertia constants and capacity factors for different generation types [17].

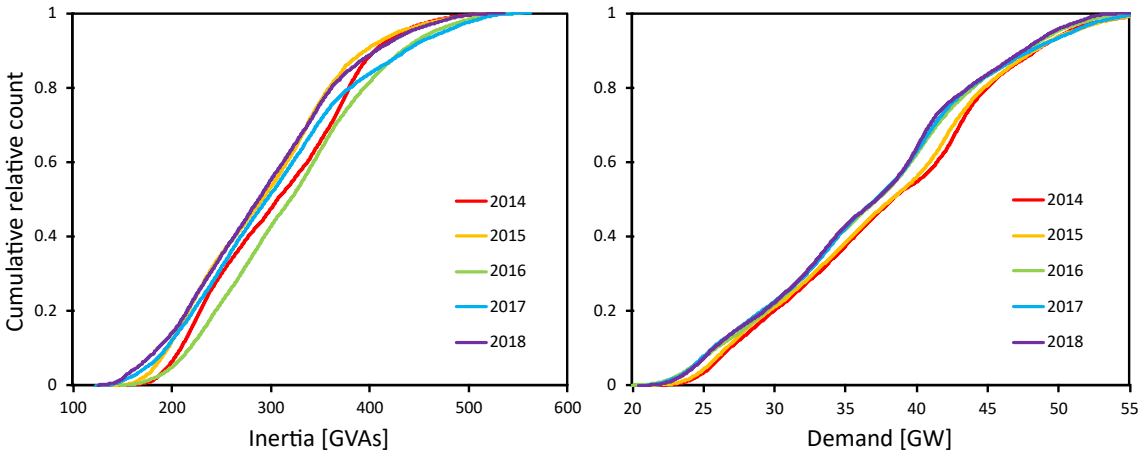

Figure 4: Cumulative distributions of inertia and demand in GB (2014–2018).

estimated capacity factors. The total inertia is therefore given by

$$\begin{aligned} E_{\mathrm{n}} &= E_{\mathrm{n,dem}} + E_{\mathrm{n,gen}} \\ &= 1.75 \times TSD + \sum_i H_i S_i \\ &= 1.75 \times TSD + \sum_i \frac{H_i P_i}{\beta_i u_i} \end{aligned} \tag{8}$$

where H_i is the inertia constant of each generation type (i), S_i is the rated capacity in MVAs, P_i is the power generation at each half-hour, u_i is the power factor, and β_i is the capacity factor. It is assumed that the power factor of all generation types that contribute inertia is 0.85. Table 1 shows the assumed inertia constants and capacity factors for each major generation type. Wind, solar, and interconnectors do not offer inertia to the grid, due to being non-synchronous, so their inertia constants are zero. This means their capacity factors are irrelevant for the purposes of calculating inertia. Nuclear has the highest capacity factor, given its use as baseload generation.

Fig. 4 shows inertia and UD cumulative distribution curves for the years 2014–2018 calculated using the above method. As can be seen, there is limited variation between the years for inertia (range of 50$^{\mathrm{th}}$ percentile is 32 GVAs) and UD (range of 50$^{\mathrm{th}}$ percentile is 1.2 GW).

FR service	Speed and duration	Aim
Primary	Delivered within 10 s and sustained for a further 20 s	To contain a falling frequency when $f < 50$ Hz
Secondary	Delivered within 30 s and sustained for a further 30 min	To restore frequency back to 50 Hz when $f < 50$ Hz
High	Delivered within 10 s and sustained indefinitely	To contain and restore frequency back to 50 Hz when $f > 50$ Hz
Enhanced (EFR)	Delivered within 1 s and sustained for 15 min	To provide fast response either side of 50 Hz (symmetric service)

Table 2: GB frequency response services [28, 33].

2.4.2. Modelling frequency response

In GB, there are 4 main types of FR service. Their exact nature and aims are presented in Table 2. Primary, secondary, and high FR are either dynamic or static: dynamic FR is the continuous provision of proportional response as the frequency changes, and static FR is a discrete service activated when the frequency passes a defined value. Enhanced FR (EFR) is a relatively new dynamic service, which is much faster acting than the other dynamic services. In 2016, GB's ESO procured 200 MW of EFR via a tender exercise [33], and all of the contracts were awarded to batteries. By summer 2018, all contracts were delivering their contracted volume.

In the GB grid model developed here, FR is modelled continuously and more accurately compared to the one-off simple representation in Fig. 3. In the model, there are 3 FR services: EFR, low FR (LFR), and high FR (HFR) based on the 4 services in Table 2. Primary and secondary FR have been combined into a single LFR service. Static FR is ignored, so all response is dynamic. EFR, LFR, and HFR have the following characteristics: deadband (± 0.015 Hz in GB [28]), delay time (t_d), response profile (required FR power output for a given frequency deviation), ramp rate, and capacity (EFR_cap, LFR_cap, and HFR_cap). The process of calculating the FR output (R) at each time step is shown in Fig. 5. The response profiles for EFR, LFR, and HFR are linear, with the maximum FR output at a ± 0.5 Hz deviation. The ramp rate limit applies to both upwards and downwards ramps.

FR is modelled as above to match the minimum requirements for FR as set out in the GB grid code [28] and the EFR delivery envelope [33]. Modelling FR in this way produces results for a worst-case scenario. In reality, some FR is delivered via governor action, which will act quicker than the FR modelled in this paper and have slightly different dynamics. Also, FR from governor action will vary slightly between different generators across the grid depending on their individual droop control settings.

LFR continues indefinitely, whereas secondary FR is only required for 30 min. This assumption is justified because frequency deviations outside of the low frequency deadband have a median

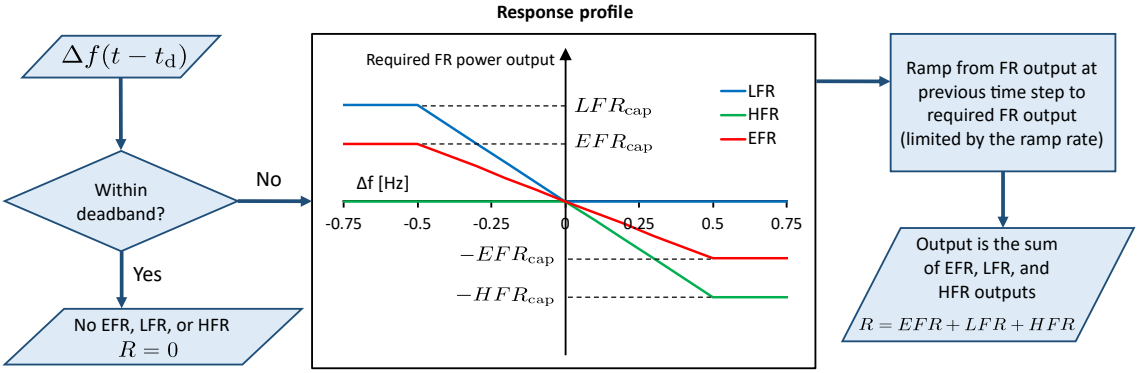

Figure 5: Process for calculating frequency response output in the GB grid model.

duration of 11 s in the time period 2014–2018 and excursions lasting over 30 min were extremely rare (0.2% of deadband excursions on the low side). With the 2014–2018 frequency data as an input, LFR would act for the same length of time as secondary FR would in the overwhelming majority of cases.

SI is modelled in this paper based on the definition in [15]. SI is a symmetric service and has a delay time of 0.2 s and ramp time of 0.2 s and is proportional to RoCoF rather than frequency deviation. The response profile for SI is similar to that presented in Fig. 5 but with $\mathrm{Hz\,s^{-1}}$ on the x axis (instead of Hz) and maximum capacity reached when RoCoF $= \pm 0.05\,\mathrm{Hz\,s^{-1}}$.

2.4.3. November 2018 case study

The GB grid model can be used to produce a historic imbalance profile by rearranging Eq. (1) so that I is the subject, as long as the other grid variables and parameters are accurately known for the time period of the simulation. In this paper, Nov18 is chosen as the case study month because in the 2014–2018 time period it has the highest frequency standard deviation of any month (0.0701) and the second highest number of frequency events (134 high, 105 low), see Fig. 7. Also, the Nov18 frequency profile never breaches 49.7 Hz or 50.3 Hz, so it is likely that no static FR was called upon during the month (these are the tightest trigger frequencies for static FR). This means that the ignoring of static FR in Section 2.4.2 does not affect the accuracy of the Nov18 imbalance calculation.

To calculate the imbalance profile for the whole month of Nov18, 1 s resolution frequency data [27] is used and the demand and inertia profiles are obtained via the method in Section 2.4.1. After fitting the GB grid model against the recent August 9$^{\mathrm{th}}$ low frequency event, we estimate the demand damping constant to be $k = 0.02$, which is the value used for Nov18. FR parameter values used in the imbalance calculation are shown in Table 3. The FR capacities for Nov18 are estimated using a Nov18 FR market report produced by the GB ESO [34]. EFR_{cap} and HFR_{cap} are constant, but LFR_{cap} varies throughout the day between three values. LFR_{cap} is based

FR service	Capacity [MW]	Delay time [s]	Ramp rate [MW s^{-1}]
EFR	200	0.5	$2EFR_{\text{cap}}$
HFR	200	2	$\frac{1}{8}HFR_{\text{cap}}$
LFR	800 (00:00–07:00) 600 (07:00–15:00) 500 (15:00-00:00)	2	$\frac{1}{8}LFR_{\text{cap}}$

Table 3: Nov18 frequency response parameter values [34, 28].

Generation type	2018 capacity [GW]	2030 (CR) capacity [GW]	Ratio
Wind (transmission)	14.7	42.2	2.87
Wind (distributed)	6.3	11.2	1.78
Solar	12.7	29.7	2.34
Nuclear	9.2	4.6	0.49

Table 4: Generation capacities in 2018 and in 2030 for the Community Renewables scenario in Future Energy Scenarios [11].

on the primary dynamic FR capacity in the report, not secondary. The secondary dynamic FR capacity in Nov18 is similar to primary, but differs slightly throughout the day. Therefore, LFR in the model accurately captures primary dynamic FR and is a reasonable estimate for secondary dynamic FR. With the delay time and ramp rates shown in Table 3, if a sudden $\Delta f = \pm 0.5\,\text{Hz}$ deviation occurred, LFR and HFR would start responding after 2 s and be at full capacity at 10 s, which matches the minimum acceptable response in Nov 2018 [28]. The time step of the grid model is 0.1 s, so all the variables mentioned are linearly interpolated during the Nov18 imbalance calculation.

In this paper, the Nov18 imbalance profile is used as an input in simulations of the GB grid model where frequency is the output. To represent future (2030) grid scenarios, simulations with the Nov18 imbalance are run with different inertia profiles (predicting a future imbalance profile is beyond the scope of this work). The method behind the creation of these profiles is explained in the next section.

2.5. November 2030 inertia profiles

The annual level of electricity demand in GB is predicted to be fairly similar in 2030 as it is now [11]. Industrial and commercial demand is expected to reduce, but this is balanced by an increase in electricity demand in the transport sector. Given this, and the difficulty in predicting an accurate demand profile for 10 years in the future, the UD in November 2030 (Nov30) is assumed to have the same profile as Nov18.

To acquire inertia profiles for Nov30, the first step is estimating a future generation mix, which is based on a publication by GB's ESO: Future Energy Scenarios [11]. Table 4 shows the

2018 capacities of wind, solar, and nuclear and the predicted 2030 capacities in the Community Renewables (CR) scenario. This scenario is chosen because it is the scenario in which wind and solar capacity increases the most. The Nov18 half-hourly generation for these generation types is multiplied by the capacity ratio in the table. Then, the difference (Q) between the sum of this generation and the Nov18 UD is calculated:

$$Q = UD - \sum_i r_i P_i \,, \tag{9}$$

where i, in this case, is only wind (transmission and distribution), solar, and nuclear. r_i is the 2030/2018 capacity ratio in Table 4. When $Q > 0$, additional generation is required to meet UD. It is beyond the scope of this study to predict what type of generation this might be, and for our purposes we are only interested in the inertia this additional generation can provide. When $Q \leq 0$, the assumption is that curtailment occurs to satisfy UD. The penetration of wind and solar (as a percentage of UD) is 23% in Nov18. The Nov30 generation mix, estimated using the method in this section, gives a wind and solar penetration of 58% (as a percentage of UD and excluding curtailed generation).

The inertia from the generation side in Nov30 is given by

$$E_{\text{n,gen}} = \begin{cases} E_{\text{n,nuclear}} + \frac{Q H_{\text{Q}}}{\beta_{\text{Q}} u_{\text{Q}}} & \text{when } Q > 0 \,, \\ E_{\text{n,nuclear}} & \text{when } Q \leq 0 \,. \end{cases} \tag{10}$$

H_{Q} is the inertia constant of the additional generation, $u_{\text{Q}} = 0.85$ is the power factor, and $\beta_{\text{Q}} = 0.75$ is the capacity factor. $E_{\text{n,nuclear}}$ is the inertia that the Nov30 nuclear generation provides, which is calculated in the exact same way as in Section 2.4.1 but multiplied by 0.49, the capacity ratio (r) for nuclear.

Table 5 shows the names of the Nov30 inertia profiles created, their demand inertia compared to Nov18 demand inertia as a ratio, their H_{Q} values, and an example generation mix for Q given the H_{Q} value. The inertia from the demand side in Nov30 is considered to be the same as Nov18 apart from in the CR30H0-75% profile, where it is reduced to 75% of the Nov18 level. Fig. 6 shows the cumulative distributions of the Nov18 and Nov30 inertia profiles. At $H_{\text{Q}} \leq 2$, for the majority of the time the inertia is lower than the lowest level reached in Nov18. At $H_{\text{Q}} = 0$, the inertia is always below 105 GVAs. The median value in the lowest inertia profile, CRH30H0-75%, is 52 GVAs. This is roughly 20% of the median of inertia in 2014–2018. In Nov18, demand inertia contributes 20% to total inertia. As H_{Q} reduces, this contribution increases: in the CR30H2 profile, demand and generation contribute inertia in equal amounts, and in the CR30H0 profile demand is contributing 75% to the total.

Profile name	Demand inertia ratio	H_Q [s]	Example generation mix for Q
CR30H8	1	8	100% CCGT
CR30H4	1	4	Similar mix to current grid
CR30H2	1	2	Mostly hydro, interconnectors, batteries, and a small amount of CCGTs.
CR30H0	1	0	All interconnectors and batteries
CR30H0-75%	0.75	0	All interconnectors and batteries

Table 5: Properties of the Nov30 inertia profiles representing future scenarios.

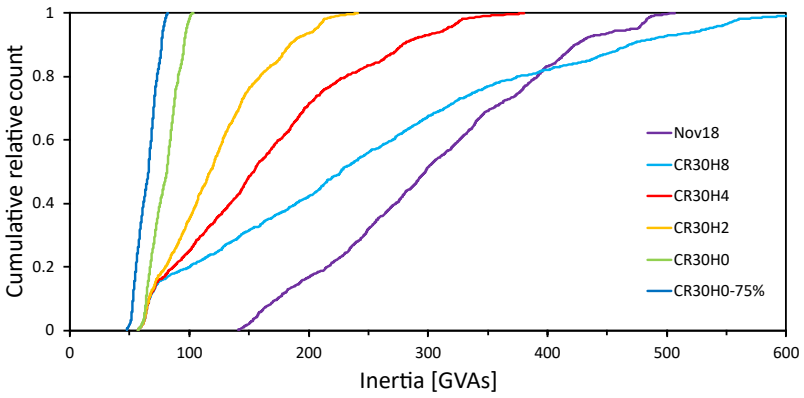

Figure 6: Cumulative distributions of the Nov30 inertia profiles in Table 5 and the Nov18 inertia profile.

3. Results and discussion

3.1. Historic GB frequency data analysis

In this section, we first present the number of frequency events and frequency standard deviation over the 5 year period analysed (2014–2018). Then, we investigate the yearly and daily temporal nature of these events. Finally, we discuss some of the results and provide possible reasons for patterns and trends observed.

Fig. 7 shows the number of events (high and low) and standard deviation each month during the 5 year period. There are no severe events during the whole time period, but 3317 high events and 1632 low events, which equates to an average of 2.7 events per day. In total, there are roughly twice as many high events as low events, and there are only 3 months where low events are more numerous. The number of events (high and low) in 2014, 2015, and 2016 are fairly similar: 708, 454, and 529, respectively. However, in 2017, this increases to 1268, and then in 2018 it increases again to 1990. There is a particularly noticeable spike at October 2017 where there are 188 high and 69 low events. The standard deviation also increases in 2017 and 2018. The standard deviation and number of events are, unsurprisingly, highly correlated ($r = 0.90$). The median event duration and magnitude does not significantly change during the 5 year time period [26].

Fig. 8 presents a heatmap of the number of events for particular months of the year and hours

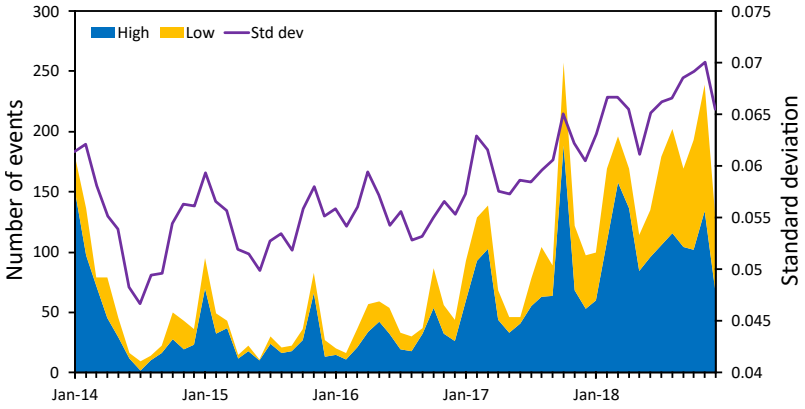

Figure 7: Number of frequency events and frequency standard deviation each month (2014–2018).

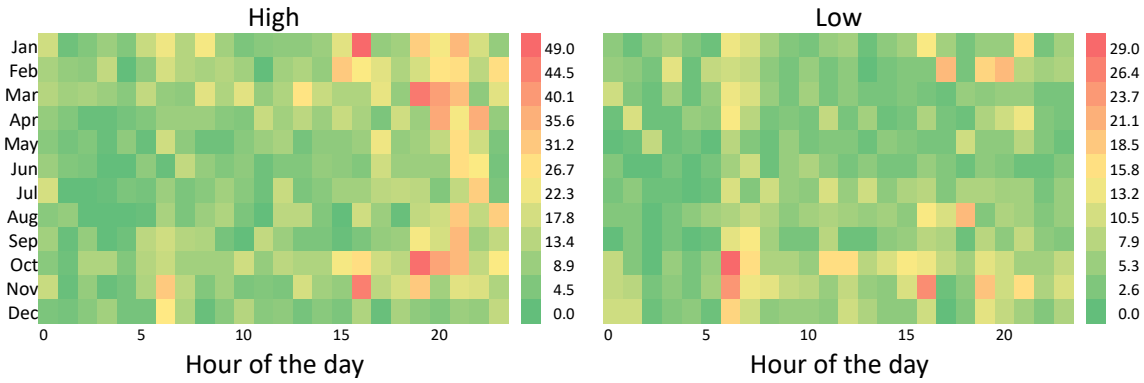

Figure 8: Number of frequency events for months of the year and hours of the day (2014–2018).

of the day during the 5 year period. There are more events in the late autumn, winter (excluding December), and early spring with fewer events in the summer. High events occur most often in the evenings (all year round) whereas low events occur most often in the mornings and autumn/winter evenings. These patterns suggest that one of the causes of frequency events is a high RoCoD (Rate of Change of Demand), since mornings and evenings are when the RoCoD is at its highest.

Over the 5 year period analysed, two thirds of events are high events. The capacity of FR that the GB ESO procures for specific times of the day is based on the level of inertia, demand, and size of the largest loss. The size of the largest loss is greater on the generation side than the demand side [29], so it follows that more dynamic primary response is procured than dynamic high response [34]. This means that when the frequency drops below 50 Hz, there is more FR delivered for a given Δf than when it goes above 50 Hz. A greater imbalance is therefore required to cause a low event than a high event, which might explain why there are fewer low events.

In GB, the electricity market is split into settlement periods (SPs). There are 48 SPs in a day, each lasting half an hour. Before the start of each SP, the GB ESO is aware of the expected generation levels and has an estimate for the demand. During the SP, generation and demand do not exactly match, so the ESO uses the Balancing Mechanism (as well as FR in real-time)

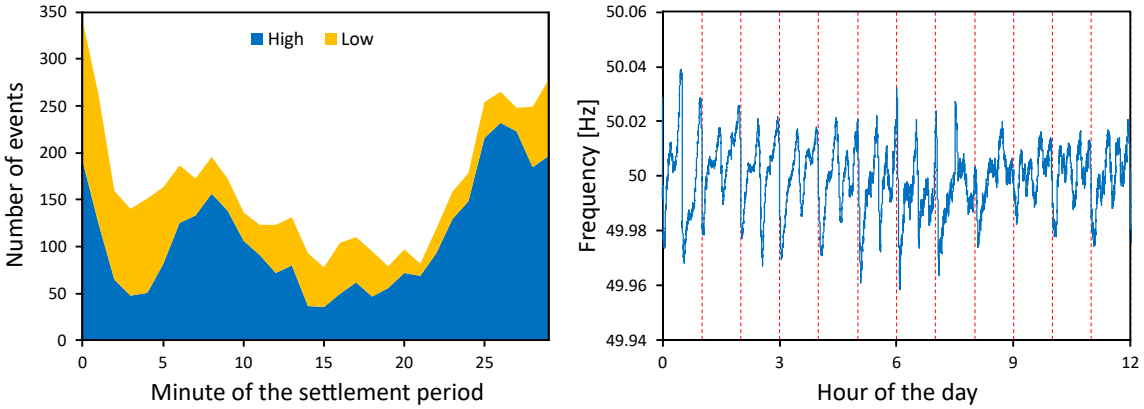

Figure 9: (left) Number of frequency events each minute of the settlement period (2014–2018). (right) Ensemble averaged frequency profile over 12 hours (2014–2019).

to increase or decrease generation or demand to ensure they are in balance. Fig. 9 (left) shows the number of frequency events at each minute of the SP (total over all SPs). The first and last minute of the SP are where the largest amount of events occur. This suggests that at the SP boundaries, generation and demand are at a greater imbalance than at other times within the SP. Fig. 9 (right) shows the ensemble averaged frequency profile over 12 hours. The profile has regular half-hourly spikes (even more pronounced on the hour), which adds further evidence that large frequency deviations occur more often at SP boundaries.

As mentioned before, Fig. 8 suggests that frequency events are correlated with RoCoD. Fig. 10 (left) shows the total number of events at each hour of the day and also the average RoCoD at each hour of the day over the 5 year period. The frequency event profile over the day has 3 spikes: one in the morning, one in the early evening, and one in the late evening. These spikes correspond to periods of high RoCoD: the morning ramp up in demand, the early evening ramp up, and the late evening ramp down. The correlation coefficient is $r = 0.72$. Fig. 10 (right) shows the total number of events at each month of the year and also the average of the average RoCoD over each month of the year over the 5 year period. There are clearly fewer events in the summer months, which is also when the average RoCoD over a month is at its lowest. The same is observed when it comes to number of events each day of the week: there are fewer events on the weekend days (average of 2 per day), where the average RoCoD over the day is lower, compared to the weekdays (average of 3 per day).

SP boundaries and RoCoD are likely causes of frequency volatility. However, this does not explain the increase in volatility during 2017 and 2018, seen in Fig. 7. SPs exist in the same way in 2017 and 2018 as they did in earlier years, and the average RoCoD each month has a slight downwards trend from 2014 to 2018 (although a seasonal pattern each year). Fig. 11 shows the penetration of wind and solar generation (as a percentage of UD) and the frequency standard deviation each month during the 5 year period. While the correlation is fairly high ($r = 0.79$), it

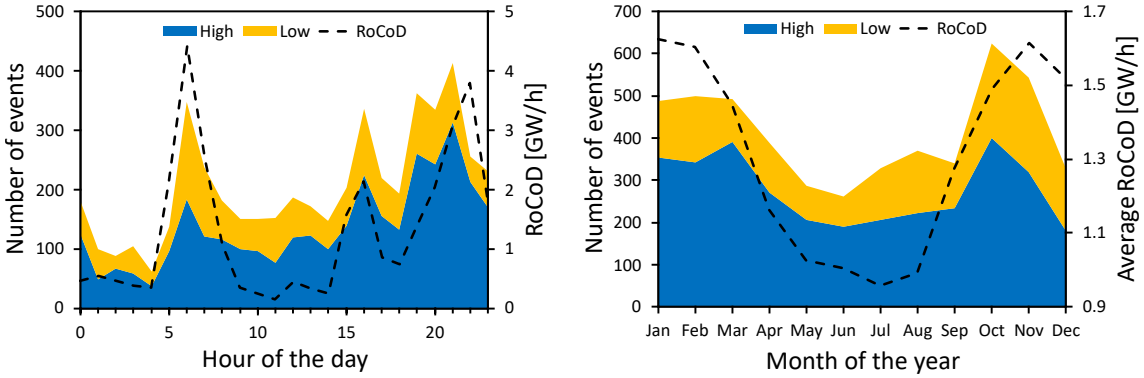

Figure 10: Number of frequency events and rate of change of demand each hour of the day and month of the year (2014–2018).

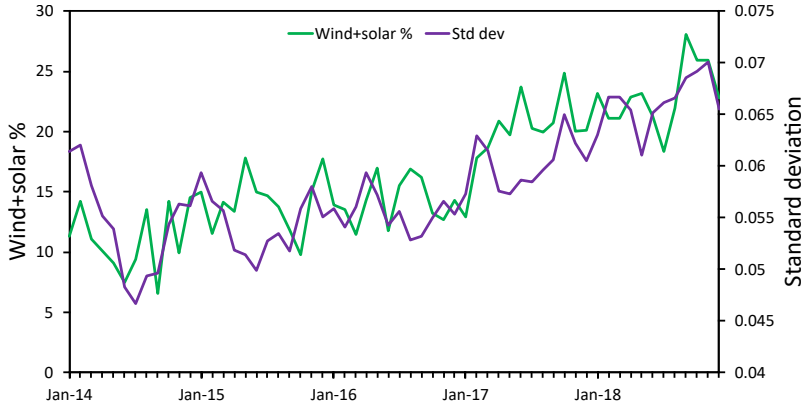

Figure 11: Wind and solar penetration and frequency standard deviation each month (2014–2018).

is impossible to say conclusively whether there is a causal relationship, though it is clear it has not been due to the lack of inertia provided by wind and solar. The inertia levels are not low enough in the 2014–2018 period to be a cause in the increase of frequency standard deviation and number of events. The correlation between total inertia and frequency standard deviation is $r = 0$ during the 5 year period. Also, between 2014 and 2018, the amount of inertia in the grid does not change by a significant amount, as can be seen in Fig. 4. The correlation between the penetration of wind and solar generation (as a percentage of UD) and the frequency standard deviation each day during the 5 year period is $r = 0.47$, much lower than the monthly correlation.

3.2. Frequency response requirements in a large infeed loss situation

In this section, we present results based on the constraints in Section 2.3, which ensure that the frequency requirements are met after a LIL of 1320 MW. $D_{\mathrm{n}} = 25.7$ GW in these results, which is the 10^{th} percentile in the 2018 demand distribution (see Fig. 4). The grid is more vulnerable to a LIL at lower demand levels, which is why a low percentile is chosen. The demand damping constant is set to 0.02 (see Section 2.4.3).

Embedded generators are equipped with loss of main (LoM) protection to protect equipment

and personnel. One common form of LoM protection is using RoCoF relays: if the relay measures a RoCoF above a set limit, the embedded generator trips offline. In the past, this RoCoF limit was $0.125\,\mathrm{Hz\,s^{-1}}$. A practical consideration is that with decreasing inertia this limit is likely to be breached during low frequency events and not LoM events, which would exacerbate the event severity. Using Eq. (5), if the inertia is below 264 GVAs, the initial RoCoF after the LIL is greater than the $0.125\,\mathrm{Hz\,s^{-1}}$ limit. From Fig. 4, we can see that this level of inertia occurs on average 36% of the time in the years 2014–2018. A change was made to the RoCoF relay limits in 2014 [35]: the limit is now $1\,\mathrm{Hz\,s^{-1}}$ (although many generators are clearly on the old setting as the August 9$^{\mathrm{th}}$ low frequency event revealed). This means that the inertia may get as low as 33 GVAs before the RoCoF limit is breached after the LIL, which is lower than the lowest value of any of the predicted Nov30 inertia profiles (see Fig. 6). For this reason, in GB, the RoCoF requirement is not likely to be the limiting factor in the future. However, this might not be the case in smaller grids around the world with lower levels of inertia and demand.

Fig. 12 (left) shows the amount of FR capacity (R_{cap}) needed against inertia for different delay times to fulfil the frequency nadir requirement, with the ramp time (t_{r}) set to 8 s. Lower inertia than shown could be reached, but we consider $R_{\mathrm{cap}} > 3000\,\mathrm{MW}$ to be impractical. Shorter delay times allow for lower inertia to be reached, but even with a 0 s delay time, the minimum inertia that can be reached is 88 GVAs. At 2 s delay time and $R_{\mathrm{cap}} = 3000\,\mathrm{MW}$, the minimum inertia that can be reached is 204 GVAs. In every Nov30 inertia profile (see Fig. 6) but one, more than 50% of time is spent with an inertia lower than this (in some profiles it is 100%).

Fig. 12 (right) shows the ramp time needed against inertia for different delay times to fulfil the nadir requirement with $R_{\mathrm{cap}} = 1063\,\mathrm{MW}$, the lowest value the FR capacity constraint (Eq. (6)) allows. The ramp time is linear with inertia and fitting a linear equation gives us this relationship:

$$t_{\mathrm{r}} = 0.0327 E_{\mathrm{n}} - 1.93 t_{\mathrm{d}}\,, \tag{11}$$

where E_{n} is in GVAs and t_{d} is in seconds. Satisfying the nadir requirement is now possible at inertia levels below 88 GVAs if $t_{\mathrm{d}} \leq 1$, but the ramp times required are very fast. For example, for a delay time of 0.5 s and an inertia of 60 GVAs, the ramp time required is 1 s. This is achievable, but only for certain generation types such as batteries and interconnectors. At $R_{\mathrm{cap}} = 1063\,\mathrm{MW}$, $t_{\mathrm{d}} = 2$, and $t_{\mathrm{r}} = 8$ (similar to current primary FR), the frequency drops lower than 48.8 Hz at an inertia level below 102 GVAs after the LIL. 48.8 Hz is the point at which demand starts to be disconnected in GB i.e. blackouts.

At inertia levels that could be common in the near future (< 100 GVAs, see Fig. 6), FR delay and ramp times need to be much shorter than they are today (excluding EFR). Currently, a large proportion of FR is provided by CCGTs. However, in the future, the delay and ramp time re-

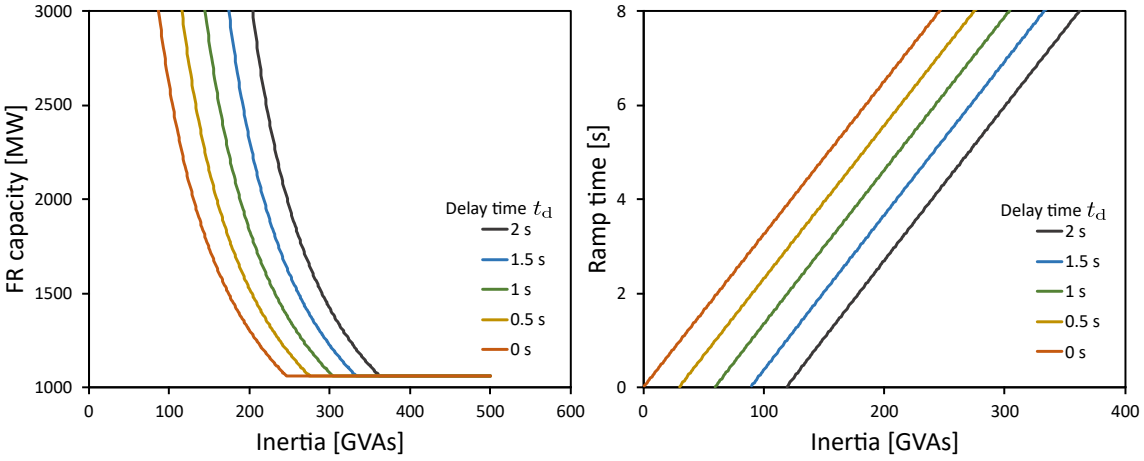

Figure 12: Frequency response capacity and ramp times necessary to ensure frequency requirements are fulfilled after the large infeed loss for different inertia levels and delay times.

quirements might necessitate the majority of FR being comprised of batteries and interconnectors, which can respond extremely fast. Increasing FR capacity could slightly relax the requirements on delay time and ramp rate, but this has a few potential issues. Firstly, it might be prohibitively expensive. Secondly, for the vast majority of time, a large proportion of the FR capacity would be redundant. Thirdly, there would be the risk of the frequency over-shooting 50 Hz during recovery after a LIL due to the combination of higher capacity and slower response speed. As another option, the frequency nadir requirement could be relaxed in the future.

3.3. Grid frequency volatility over a month in future scenarios

The Nov18 imbalance profile and results from the month-long simulations of frequency with future (2030) inertia profiles are presented in Section 3.3.1 and Section 3.3.2, respectively.

3.3.1. November 2018 imbalance

Fig. 13 shows the imbalance distribution for Nov18. The distribution has a peak at −80 MW and another peak at 40 MW. There is a longer tail on the negative imbalance side: at any imbalance magnitude above roughly 140 MW, there are more counts in the negative bin than the corresponding positive bin. The normalised count at either end, −700 MW and 500 MW, is $\approx 10^{-5}$.

The imbalance reaches a low of −766 MW and a high of 563 MW during the month. The −766 MW low is reached during a sudden drop from 64 MW ($\Delta I = -830$ MW), which causes a frequency drop from 50.052 Hz to the minimum frequency of the month, 49.701 Hz. The 563 MW high causes a frequency of 50.243 Hz, which is almost as high as the maximum frequency of the month, 50.291 Hz.

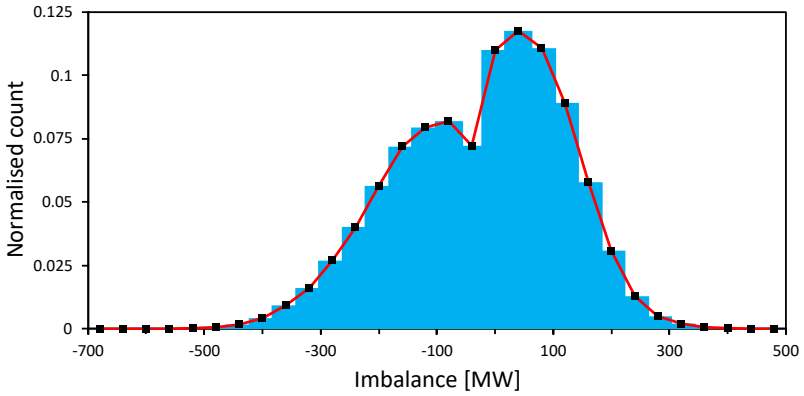

Figure 13: Imbalance distribution in Nov18. Bin width: 40 MW.

3.3.2. November 2030 inertia profiles

Fig. 14 shows the frequency standard deviation and number of events for 5 month-long frequency simulations with the different Nov30 inertia profiles in Fig. 6 and Table 5 (and Nov18 for comparison). In these 5 simulations there is no EFR, but LFR_{cap} and HFR_{cap} are 200 MW higher than their Nov18 value so the overall FR capacity is the same as Nov18. As H_{Q} reduces, the standard deviation and number of events increase steadily. At no point are there any severe frequency events. However, with the CR30H0-75% profile, the frequency minimum and maximum are 49.536 Hz and 50.469 Hz, respectively. There is a large difference between the CR30H0 and CR30H0-75% profiles. At this level of inertia, where only nuclear (on the generation side) and demand (at 75% of the Nov18 level) are contributing, the frequency volatility is definitely not acceptable. The low inertia is causing the frequency to change faster than the FR can effectively keep up with. One thing to note is that at a demand inertia of 75% of the Nov18 level, fewer synchronous demand units are likely to be connected to the grid (or smaller in size). This would almost certainly have a detrimental effect on the demand damping of the grid, a self-stabilising property, causing far greater volatility in the frequency. Quantifying this detrimental effect is beyond the scope of this study.

Various low inertia mitigation methods are investigated to see which approach is able to bring the frequency volatility back into an acceptable range for the CR30H0-75% inertia profile. The results are shown in Table 6. The first method, *Increase LFR/HFR*, is simply increasing the LFR/HFR capacity by 200 MW, which results in a lower frequency standard deviation but a massive increase in the number of events, especially on the low side (also 20 severe low events). The increased FR capacity is not beneficial and is actually detrimental because there is now more response acting at occasionally unsuitable times. With the *Faster LFR/HFR* method, the delay time of LFR/HFR is halved to 1 s and the ramp rate of LFR and HFR doubled. This reduces both the standard deviation and number of events, especially on the low side. However, the standard

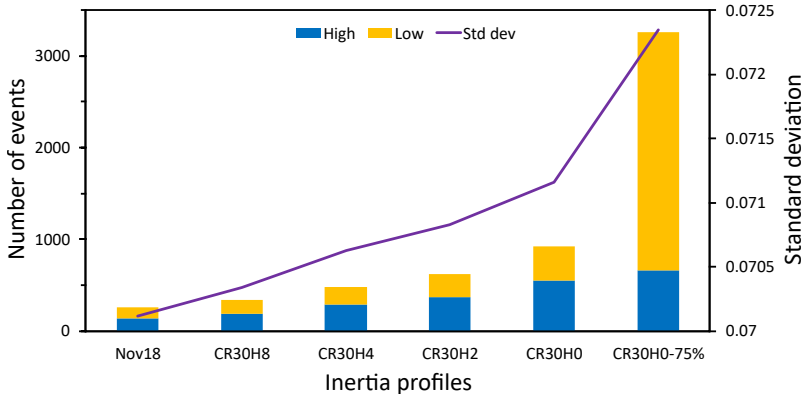

Figure 14: The effect of changing inertia (using Nov30 inertia profiles) on the number of frequency events and frequency standard deviation over a month.

	Capacity [MW]				Events	
Mitigation method	LFR/HFR	EFR	SI	Std dev	High	Low
None	Nov18 + 200	0	0	0.0723	662	2597
Increase LFR/HFR	Nov18 + 400	0	0	0.0693	1220	12641
Faster LFR/HFR	Nov18 + 200	0	0	0.0710	619	415
With SI	Nov18	0	200	0.0895	2043	1036
With EFR	Nov18	200	0	0.0711	624	410
More EFR + SI	Nov18	300	100	0.0641	157	103

Table 6: Frequency volatility over a month with the CR30H0-75% (lowest inertia) profile with various low inertia mitigation methods.

deviation and the number of events are still a lot higher compared to what they were in Nov18. For the *With SI* method, 200 MW of SI replaces 200 MW of LFR/HFR (with the LFR/HFR delay time and ramp rates back at Nov18 values). The SI does not act as a good substitute for FR and the frequency volatility is unacceptable. The *With EFR* method is the same as the previous one but with 200 MW of EFR instead of SI. Results are similar to the *Faster LFR/HFR* method, suggesting that only a portion of FR needs to be fast responding to see improvements. The last mitigation method, *More EFR + SI*, is the same as the previous one but with an extra 100 MW of EFR and 100 MW of SI. In this case, the SI and extra FR capacity has a beneficial effect, unlike in *With SI* and *Increase LFR/HFR*, because there is fast acting FR (EFR) present. For the CR30H0-75% inertia profile, this mitigation method has brought the frequency volatility back into an acceptable range.

For all of the month-long simulations that produce acceptable frequency volatility, the minimum total FR delivery volume is 51 GWh, which equates to an average of 70 MW of FR being delivered at each point in time. This means that for the majority of time there is a lot of FR capacity that is not being used. If an FR service had a maximum output at smaller frequency deviations (e.g. 0.2 Hz rather than 0.5 Hz) then all of the capacity would be utilised more often. Other FR services

would be needed to manage the frequency for times when the deviations are larger e.g. post-fault.

4. Conclusions

From our analysis of historic GB frequency data, we have shown that frequency volatility in GB increased substantially in 2017 and then again in 2018. We have also shown that the main drivers behind volatility, in general, are SP boundaries and high RoCoD. With a fixed FR capacity, we found a relationship between inertia and FR delay and ramp times to ensure frequency requirements are satisfied after a LIL. Full FR response needs to be delivered within a few seconds at inertia levels below 100 GVAs, assuming a LIL of 1320 MW. In 2030, the average inertia of the grid will likely be lower than today, but we found that very low levels need to be reached before frequency volatility starts to be seriously affected in normal day-to-day operation. In the most extreme low inertia scenario modelled (CR30H0-75%), inertia was only provided by nuclear generation and demand and was around 20% of current levels. In this extreme case, the frequency volatility was unacceptable, but it was found that adding a small amount of SI and FR capacity together with substituting some slow acting FR with fast acting FR successfully mitigated this. The proportion of fast acting FR is roughly 50% of the total capacity in this scenario.

By studying both a LIL situation and day-to-day frequency volatility we have shown that as the inertia of the grid decreases, the difference between the FR capacity needed to secure the grid against LILs and what is needed during normal day-to-day operation increases. The same can be said of FR response speeds. If frequency requirements are relaxed or the LIL is reduced in future, the difference will be less pronounced. Another solution to this could be the ESO utilising storage capacity within the EV fleet during LIL situations to temporarily increase the FR capacity when needed.

It is clear, whether looking at normal day-to-day operation or a LIL, that a significant part of the total FR capacity in the future will have to be fast acting (similar to EFR). This could be provided by batteries and interconnectors but not from common FR generation types such as hydro and CCGTs because their response times are not fast enough.

Acknowledgements

The authors gratefully acknowledge the financial support of the Engineering and Physical Sciences Research Council (EPSRC) via grant EP/L016818/1 which funds the Centre for Doctoral Training in Energy Storage and its Applications. In addition, the authors thank RWE Generation UK for their project sponsorship and support.

Bibliography

[1] US Department of Energy, "Maintaining Reliability in the Modern Power System," 2016.

[2] ENTSO-E, "Frequency Stability Evaluation Criteria for the Synchronous Zone of Continental Europe," 2016.

[3] National Grid ESO, "Technical Report on the events of 9 August 2019," 2019.

[4] G. Andersson, P. Donalek, R. Farmer, N. Hatziargyriou, I. Kamwa, P. Kundur, N. Martins, J. Paserba, P. Pourbeik, J. Sanchez-Gasca, R. Schulz, A. Stankovic, C. Taylor, and V. Vittal, "Causes of the 2003 Major Grid Blackouts in North America and Europe, and Recommended Means to Improve System Dynamic Performance," *IEEE Transactions on Power Systems*, vol. 20, no. 4, pp. 1922–1928, 2005.

[5] AEMO, "Black System South Australia," 2017.

[6] P. Kundur, *Power System Stability and Control*. McGraw-Hill, 1994.

[7] United Nations Framework Convention on Climate Change (UNFCCC), "Paris Agreement," 2015.

[8] UK Parliament, "Climate Change Act 2008," 2008.

[9] International Energy Agency (IEA), "Tracking Clean Energy Progress," 2017.

[10] UK Government (BEIS), "Digest of United Kingdom Energy Statistics 2018," 2018.

[11] National Grid ESO, "Future Energy Scenarios," 2019.

[12] National Grid, "Product Roadmap for Frequency Response and Reserve," 2017.

[13] A. Ulbig, T. S. Borsche, and G. Andersson, "Impact of low rotational inertia on power system stability and operation," in *19th IFAC World Congress*, (Cape Town, South Africa), 2014.

[14] P. Tielens and D. Van Hertem, "The relevance of inertia in power systems," *Renewable and Sustainable Energy Reviews*, vol. 55, pp. 999–1009, 2016.

[15] R. Eriksson, N. Modig, and K. Elkington, "Synthetic inertia versus fast frequency response: a definition," *IET Renewable Power Generation*, vol. 12, no. 5, pp. 507–514, 2018.

[16] Q. Hong, M. Nedd, S. Norris, I. Abdulhadi, M. Karimi, V. Terzija, B. Marshall, K. Bell, and C. Booth, "Fast frequency response for effective frequency control in power systems with low inertia," *The Journal of Engineering*, vol. 2019, no. 16, pp. 1696–1702, 2019.

[17] R. Lee, S. Homan, N. Mac Dowell, and S. Brown, "A closed-loop analysis of grid scale battery systems providing frequency response and reserve services in a variable inertia grid," *Applied Energy*, vol. 236, no. December 2018, pp. 961–972, 2019.

[18] D. M. Greenwood, K. Y. Lim, C. Patsios, P. F. Lyons, Y. S. Lim, and P. C. Taylor, "Frequency response services designed for energy storage," *Applied Energy*, vol. 203, pp. 115–127, 2017.

[19] S. C. Johnson, D. J. Papageorgiou, D. S. Mallapragada, T. A. Deetjen, J. D. Rhodes, and M. E. Webber, "Evaluating rotational inertia as a component of grid reliability with high penetrations of variable renewable energy," *Energy*, vol. 180, pp. 258–271, 2019.

[20] S. C. Johnson, J. D. Rhodes, and M. E. Webber, "Understanding the impact of non-synchronous wind and solar generation on grid stability and identifying mitigation pathways," *Applied Energy*, vol. 262, no. 114492, 2020.

[21] P. Vorobev, D. Greenwood, J. H. Bell, J. W. Bialek, P. C. Taylor, and K. Turitsyn, "Deadbands, Droop and Inertia Impact on Power System Frequency Distribution," *IEEE Transactions on Power Systems*, vol. 34, no. 4, pp. 3098–3108, 2019.

[22] P. J. Vogler-Finck and W. G. Früh, "Evolution of primary frequency control requirements in Great Britain with increasing wind generation," *International Journal of Electrical Power and Energy Systems*, vol. 73, pp. 377–388, 2015.

[23] P. V. Brogan, R. J. Best, D. J. Morrow, K. McKinley, and M. L. Kubik, "Effect of BESS Response on Frequency and RoCoF During Underfrequency Transients," *IEEE Transactions on Power Systems*, vol. 34, no. 1, pp. 575–583, 2019.

[24] H. Wyman-Pain, Y. Bian, and F. Li, "Changes in Frequency Events and the Frequency Response Markets in Great Britain," in *IEEE Power & Energy Society General Meeting*, (Portland, USA), IEEE, 2018.

[25] B. Schäfer, C. Beck, K. Aihara, D. Witthaut, and M. Timme, "Non-Gaussian power grid frequency fluctuations characterized by Lévy-stable laws and superstatistics," *Nature Energy*, vol. 3, no. 2, pp. 119–126, 2018.

[26] S. Homan and S. Brown, "An analysis of frequency events in Great Britain," *Energy Reports*, pp. 63–69, 2020.

[27] National Grid ESO, "Data finder and explorer." Available at: https://www.nationalgrideso.com/balancing-data/data-finder-and-explorer. [Accessed: 11-Feb-20].

[28] National Grid, "The Grid Code," 2018.

[29] National Grid, "System Security and Quality of Supply Standard," 2019.

[30] Elexon, "Balancing mechanism reports." Available at: https://www.bmreports.com/bmrs/?q=generation/fueltype. [Accessed: 11-Feb-20].

[31] P. M. Ashton, C. S. Saunders, G. A. Taylor, A. M. Carter, and M. E. Bradley, "Inertia estimation of the GB power system using synchrophasor measurements," *IEEE Transactions on Power Systems*, vol. 30, no. 2, pp. 701–709, 2015.

[32] Y. Bian, H. Wyman-Pain, F. Li, R. Bhakar, S. Mishra, and N. Prasad Padhy, "Demand Side Contributions for System Inertia in the GB Power System," *IEEE Transactions on Power Systems*, vol. 33, no. 4, pp. 3521–3530, 2018.

[33] National Grid, "Enhanced frequency response: Invitation to tender for pre-qualified parties," 2016.

[34] National Grid ESO, "Firm Frequency Response (FFR) Market Information Report for Nov-18," 2018.

[35] Ofgem, "Changes to the Distribution Code and Engineering Recommendation G59: Frequency Changes during Large Disturbances and their Impact on the Total System," 2014.